Acta Mechanica Solida Sinica, Vol. 33, No. 3, June, 2020, 392–402 ISSN 1860-2134
https://doi.org/10.1007/s10338-019-00154-y

Strain Amplitude Effect on the Viscoelastic Mechanics of Chloroprene Rubber

Longfan Peng[1*] **Zhida Li**[1] **Yunyu Li**[1]
([1] *Institute of Transportation, Wuhan University of Technology, Wuhan 430063, Hubei, China*)

Received 26 March 2019; revision received 30 October 2019; Accepted 5 November 2019;
published online 21 November 2019
© The Chinese Society of Theoretical and Applied Mechanics 2019

ABSTRACT This paper establishes an empirical formula to predict the strain amplitude effect. A viscoelastic constitutive model—the superposition of a hyperelastic model and a viscoelastic model—is constructed based on the laws of thermodynamics. The Mooney–Rivlin model and the Prony series are employed for uniaxial tension testing. The empirical formula is derived using a hysteresis loop; it obtains results that are in agreement with the experimental results of dynamic mechanical analysis (DMA). The empirical formula proposed in this paper has certain accuracy in predicting the dynamic modulus under different strain amplitudes.

KEY WORDS Viscoelasticity, Strain amplitude effect, Storage modulus, Loss modulus, Hysteresis loop

1. Introduction

Filled rubber materials, such as carbon black or silica, are widely used in automobiles, machines, and buildings owing to their superior elastic and damping properties [1–6]. These materials exhibit mechanical properties such as hyperelasticity and viscoelasticity. Similar to the Mullins effect [7–9], reversible softening was observed with an increase in strain amplitude, known as the Payne effect [10]. The Payne effect is related to filler–filler and filler–rubber interactions, and can be described as the breakage and recovery of the network during cyclic loading. Among the specifically developed models, the Kraus model [11] is based on microstructural destruction and reorganization rates of the carbon black network. The modeling results fit the test data without any time-domain formulation, while the material parameters need reidentification if the frequency changes. Luo [12] further extended the Kraus model and used it to model frequency- and amplitude-dependent dynamic modulus and hysteresis loss. Lion [13–15] developed a time-domain formulation valid for arbitrary deformation and employed a constitutive model using a series of nonlinear Maxwell elements. Youn [16] extended the Kraus model to consider a large static pre-strain. Tomita [17] further proposed a visco–hyperelastic eight-chain network model that incorporates a nonlinear dashpot with Langevin springs.

As a standard experimental approach, the dynamic mechanical analysis (DMA) is very helpful for studying these effects. In DMA, an oscillating elongation is applied to the sample and the response of the material is analyzed as a force signal, which includes all material nonlinearities. The processing of these signals allows computing new dynamic measures known as the dynamic modulus. Further, considering time signals is very helpful for investigating transient effects in the time domain directly.

* Corresponding author. E-mail: plf_ayusuke@163.com

This paper first builds a nonlinear constitutive model of chloroprene rubber considering the strain amplitude effect, which is specified by the Mooney–Rivlin model and Prony series under uniaxial tension. Second, with the DMA test results, an empirical formula of the loss modulus is obtained from the hysteresis loop to predict the strain amplitude effect. Finally, the storage modulus is fitted by the same expression as that for the loss modulus. The proposed empirical formula has certain accuracy in predicting the dynamic modulus under different strain amplitudes for both the storage modulus and the loss modulus, and it can be further expressed in a simple form.

2. Dynamic Characteristics

2.1. General Theory

The time-dependent vector function $x = \chi(X, t)$ is defined as the time-dependent mapping between the position vector $X(P)$ of the reference configuration and the position vector $x(P)$ of the current configuration. The deformation gradient $F(t)$ at the current time t is written as

$$F(t) = \mathrm{Grad}(\chi(X, t)) = \frac{\partial x}{\partial X} \tag{1}$$

The relative deformation gradient in Cartesian coordinates is defined as

$$F_t(s) = F(s)F^{-1}(t) 0 \leq s \leq t \tag{2}$$

The deformation gradient tensor $F(t)$ maps the material tangent vectors from the current configuration at time t to the tangent vectors at previous time s. The right and left Cauchy–Green deformation tensors C and B are separately defined as

$$C = F^T F,\ B = FF^T \tag{3}$$

Further, the Piola and Green–Lagrange strain tensors e and E are defined as

$$e = \frac{1}{2}(C^{-1} - I), \quad E = \frac{1}{2}(C - I) \tag{4}$$

Using Eq. (2), the relative right Cauchy–Green deformation tensor is expressed as

$$C_t(s) = F_t^T(s)F_t(s) = F^{-T}(t)C(s)F^{-1}(t) \tag{5}$$

and the relative Piola and Cauchy–Green strain tensors are

$$e_t(s) = \frac{1}{2}(C_t^{-1}(s) - \mathrm{I}),\ \mathrm{E}_t(s) = \frac{1}{2}(\mathrm{C}_t(s) - \mathrm{I}) \tag{6}$$

Equations (5) and (6) have the properties

$$E_t(s) = e_t(s) = 0, \quad \mathrm{d}/\mathrm{d}s(E_t(s) \cdot 1) = E'(s) \cdot C^{-1}(t) \text{ and } \mathrm{d}/\mathrm{d}s(e_t(s) \cdot 1) = e'(s) \cdot C(t) \tag{7}$$

As rubber-like materials exhibit mechanical properties such as hyperelasticity and viscoelasticity, the Helmholtz free energy per unit reference volume W depends not only on the Cauchy–Green deformation tensor C, but also on the rate of Cauchy–Green strain tensor $\dot{E}$, which is the sum of two parts

$$\begin{aligned} W &= W(C, \dot{E}) = W_e(C) + W_v(C, \dot{E}, \eta_i) \\ &= W_e(I_1, I_2, I_3, C_j) + \frac{1}{2}(E_L(\eta_i, t) * \dot{E}) : C \\ &= W_e(I_1, I_2, I_3, C_j) + \frac{1}{2}\left[\int_0^t E_L(\eta_i, t - \tau)\dot{E}(\tau)\mathrm{d}\tau\right] : C \end{aligned} \tag{8}$$

where W_e represents the elastic strain energy density corresponding to the equilibrium state; $W_e(C)$ is obtained from hyperelastic parameters C_j and three independent invariants I_1, I_2, and I_3 of the right Cauchy–Green deformation tensor C; $W_v(C, \dot{E})$ is the viscous dissipation of the solid during the mechanical response; E_L is the relaxation function; the notation ":" denotes the contraction over two tensors A and B ($A : B = A_{ij}B_{ij}$); and the symbol "*" represents the convolution integral between two functions $f(t)$ and $g(t)$ (i.e., $f * g = \int_0^t f(t - \tau)g(\tau)\mathrm{d}\tau$).

As the rubber-like material is considered incompressible, the independent invariant I_3 equals 1; thus, Eq. (8) becomes

$$\begin{aligned} W &= W(C,\dot{E}) = W_e(C) + W_v(C,\dot{E},\eta_i) \\ &= W_e(I_1,I_2,C_{\mathrm{j}}) + \frac{1}{2}\left[E_L(\eta_i,t) * \dot{E}\right] : C \end{aligned} \tag{9}$$

Then, the Clausius–Duhem inequality is written in the alternative form

$$\frac{1}{2}T : \dot{C} - \dot{W} - s\dot{T} - \frac{q}{T} \cdot \nabla T \geq 0 \tag{10}$$

where T is the second Piola–Kirchhoff stress tensor, and s and q are the entropy and heat flux flowing outside the material, respectively.

Substituting Eq. (9) into Eq. (10), and considering the isothermal process, the total energy dissipation rate $\dot{D}$ can be derived as

$$\begin{aligned} \dot{D} = &\left(T + pC^{-1} - 2\left(\frac{\partial W_e}{\partial I_1} + I_1\frac{\partial W_e}{\partial I_2}\right)I + 2\frac{\partial W_e}{\partial I_2}C - E_L * \dot{E}\right) : \frac{\dot{C}}{2} - \frac{1}{2}\left(\frac{\partial E_L}{\partial t} * \dot{E} + E_L(\eta_i,0)\dot{E}(t)\right) : C \\ &- \sum_{j=1}^{m}\frac{\partial W_e}{\partial C_j}\dot{C}_j - \sum_{i=1}^{n}\frac{\eta_i}{2}\left(\frac{\partial E_L}{\partial \eta_i} * \dot{E}\right) : C \geq 0 \end{aligned} \tag{11}$$

where p is a multiplier representing hydrostatic pressure that could be determined from the boundary conditions.

When the current stretch does not exceed the maximum reached in the loading, $\dot{C}_j$ and $\dot{\eta}_i$ equal to zero, i.e., the third and fourth terms of Eq. (11) vanish. The first term of $\dot{D}$ vanishes if an instantaneous mechanical balance is assumed for any arbitrary $\dot{C}$, and then, the second Piola–Kirchhoff stress tensor is written as

$$T = -pC^{-1} + 2\left(\frac{\partial W_e}{\partial I_1} + I_1\frac{\partial W_e}{\partial I_2}\right)I - 2\frac{\partial W_e}{\partial I_2}C + E_L * \dot{E} \tag{12}$$

Considering the relationship between Cauchy stress and the second Piola–Kirchhoff stress, Eq. (12) can be expressed as

$$\sigma = -pI + 2\left(\frac{\partial W_e}{\partial I_1} + I_1\frac{\partial W_e}{\partial I_2}\right)B - 2\frac{\partial W_e}{\partial I_2}B^2 + F(E_L * \dot{E})F^T. \tag{13}$$

The second term represents the energy loss rate caused by the viscosity of the rubber-like materials.

$$\dot{D}_v = -\frac{1}{2}\left(\frac{\partial E_L}{\partial t} * \dot{E} + E_L(\eta_i,0)\dot{E}(t)\right) : C. \tag{14}$$

2.2. Dynamic Modulus under Tension

In the DMA test, the material is subjected to a harmonic strain $\varepsilon_1 \sin\omega t$ with a given pre-strain ε_0; thus, the deformation gradient F, the left Cauchy–Green strain tensor B, and the rate of the Green–Lagrange strain tensor $\dot{E}$ are given as

$$[F] = \begin{bmatrix} \lambda & 0 & 0 \\ 0 & 1/\sqrt{\lambda} & 0 \\ 0 & 0 & 1/\sqrt{\lambda} \end{bmatrix} \quad [B] = \begin{bmatrix} \lambda^2 & 0 & 0 \\ 0 & 1/\lambda & 0 \\ 0 & 0 & 1/\lambda \end{bmatrix} \quad \left[\dot{E}\right] = \begin{bmatrix} \lambda\dot{\lambda} & 0 & 0 \\ 0 & -\frac{1}{2}\lambda^{-2}\dot{\lambda} & 0 \\ 0 & 0 & -\frac{1}{2}\lambda^{-2}\dot{\lambda} \end{bmatrix} \tag{15}$$

Using the Mooney–Rivlin and the generalized Maxwell models to describe the hyperelastic and viscoelastic characteristics separately, W_e and W_v are expressed as

$$W_e = C_1(I_1 - 3) + C_2(I_2 - 3) \tag{16}$$

$$W_v = \frac{1}{2}\left[\sum_{i=1}^{n} E_i \mathrm{e}^{-t/\tau_i} * \dot{E}(t)\right] : C \tag{17}$$

Substituting Eqs. (15), (16), and (17) into Eq. (13), the constitutive relationship between the stresses and the stretch are

$$\sigma_{11} = -p + 2\left[C_1 + (\lambda^2 + 2\lambda^{-1})C_2\right]\lambda^2 - 2C_2\lambda^4 + \lambda^2\left[\sum_{i=1}^{n} E_i \mathrm{e}^{-t/\tau_i} * (\lambda\dot{\lambda})\right] \tag{18}$$

$$\sigma_{22} = -p + 2\left[C_1 + (\lambda^2 + 2\lambda^{-1})C_2\right]\lambda^{-1} - 2C_2\lambda^{-2} - \frac{\lambda^{-1}}{2}\left[\sum_{i=1}^{n} E_i \mathrm{e}^{-t/\tau_i} * (\lambda^{-2}\dot{\lambda})\right] \tag{19}$$

Since the tension experiments are adopted, and the boundary conditions $\sigma_{22} = 0$ are considered, the hydrostatic pressure is obtained as

$$p = 2\left[C_1 + (\lambda^2 + 2\lambda^{-1})C_2\right]\lambda^{-1} - 2C_2\lambda^{-2} - \frac{\lambda^{-1}}{2}\left[\sum_{i=1}^{n} E_i \mathrm{e}^{-t/\tau_i} * (\lambda^{-2}\dot{\lambda})\right] \tag{20}$$

Thus, the uniaxial stress can be written as

$$\sigma_{11} = 2(\lambda^2 - \lambda^{-1})C_1 + 2(\lambda + \lambda^{-2})C_2 + \lambda^2\left[\sum_{i=1}^{n} E_i \mathrm{e}^{-t/\tau_i} * (\lambda\dot{\lambda})\right] + \frac{\lambda^{-1}}{2}\left[\sum_{i=1}^{n} E_i \mathrm{e}^{-t/\tau_i} * (\lambda^{-2}\dot{\lambda})\right] \tag{21}$$

The relationship between the stretch and the strain is given as

$$\lambda = 1 + \varepsilon_0 + \varepsilon_1 \sin\omega t = \lambda_0(1 + \hat{\varepsilon}\sin\omega t) \tag{22}$$

with

$$\hat{\varepsilon} = \frac{\varepsilon_1}{1 + \varepsilon_0} \tag{23}$$

As the dynamic strain is usually small to be regarded as $\varepsilon_1 \ll 1$, which means $\hat{\varepsilon} \ll 1$ as well. Neglecting the transient and higher-order terms, Eq. (21) becomes

$$\sigma_{11} = 2(\lambda_0^2 - \lambda_0^{-1})C_1 + 2(\lambda_0 + \lambda_0^{-2})C_2 + E'\hat{\varepsilon}\sin\omega t + E''\hat{\varepsilon}\cos\omega t \tag{24}$$

The storage modulus and loss modulus are, respectively, given as

$$\begin{aligned} E' &= E_0 + \sum_{i=1}^{n} E_i \frac{(1 + 2\lambda_0^6)\omega^2\tau_i^2}{2\lambda_0^2(1 + \omega^2\tau_i^2)} \\ &= 2(2\lambda_0^2 + \lambda_0^{-1})C_1 + 2(\lambda_0 + 2\lambda_0^{-2})C_2 + \sum_{i=1}^{n} E_i \frac{(1 + 2\lambda_0^6)\omega^2\tau_i^2}{2\lambda_0^2(1 + \omega^2\tau_i^2)} \end{aligned} \tag{25}$$

$$E'' = \sum_{i=1}^{n} E_i \frac{(1 + 2\lambda_0^6)\omega\tau_i}{2\lambda_0^2(1 + \omega^2\tau_i^2)}. \tag{26}$$

2.3. Hysteresis Loss and Energy Dissipation

When a viscoelastic material is subjected to a sinusoidal excitation under tension, the mechanical energy absorbed per unit volume of the material in the deformation up to time t is given by

$$W(t) = \int_0^t \sigma_{11}(\tau)\dot{\varepsilon}_{11}(\tau)\mathrm{d}\tau \tag{27}$$

The amount of energy dissipated [18–21] in a full cycle of oscillatory straining can be calculated by integrating Eq. (27) over the cycle.

$$D_v = \int_0^{\frac{2\pi}{\omega}} \sigma_{11}(\tau)\dot{\varepsilon}(\tau)\mathrm{d}\tau = \pi\varepsilon_1^2 E'' \tag{28}$$

Fig. 1. DMA, Gabo Eplexor 500 N

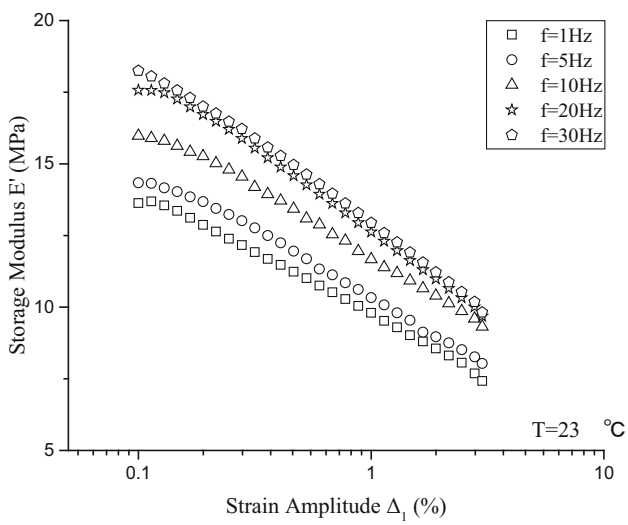

Fig. 2. Storage modulus under amplitude sweep

3. Experiment, Results, and Discussion

3.1. Experiment

Rectangular specimens with dimensions of 5 mm × 25 mm × 2 mm were selected for the test. These specimens were provided by the Dongxin rubber company in Hengshui, Hebei, China. The amplitude sweep experiment of chloroprene rubber was measured using a dynamic mechanical analyzer (DMA, Gabo Eplexor 500 N), as shown in Fig. 1.

Repeated cyclic stretching was carried out on specimens before the experiment to ensure that the stress was within the range of linear viscoelasticity during the experiment, and the Mullins effect was removed. The specimens were sinusoidally stretched under a pre-strain of 5% at various frequencies (1, 5, 10, 20, and 30 Hz); the dynamic strain amplitude ranges from 0.1% to 3% and is linearly distributed in logarithmic coordinates. The stress responses to the strain excitations were recorded automatically; the tensile storage modulus and the loss modulus were calculated from these measurements; and the mechanical hysteresis loop in a full strain cycle was also constructed.

3.2. Results

The test results are shown in Figs. 2 and 3, where the storage and loss moduli are shown as a function of the applied frequency and strain amplitude. The results indicate that the storage modulus decreases

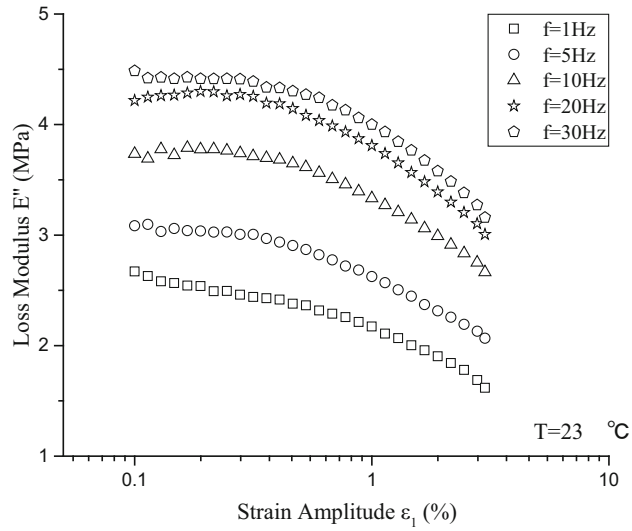

Fig. 3. Loss modulus under amplitude sweep

with an increase in strain amplitude, while the loss modulus does not show a peak value, which are similar to the experimental results in [22]. These results are attributed to the filler–filler and filler–rubber interactions.

Figure 4 shows the hysteresis loops of the material under different frequencies and strain amplitudes. The area of the hysteresis loop represents the energy dissipated in a full deformation cycle, each of which is obtained by numerical integration.

Figure 5 shows the integration results at the specified frequency and strain amplitude. It can be easily determined that hysteresis increases with an increase in the strain amplitude, and it has weak dependency on the frequency. Compared with the test results, the calculation results of Eq. (28) are relatively close.

3.3. Discussion

Figure 5a indicates that in the double logarithmic coordinate system, there is a linear relationship between the hysteresis loss and the strain amplitude, implying that the hysteresis loss and strain amplitude have a power-law relationship. The $\log D_v \sim \log \varepsilon_1$ curves are parallel and linear, which overlap after a vertical shift. Therefore, there is a vertical shift factor, which satisfies the shift relation,

$$D_v(f, \varepsilon_1) = \varphi_f D_v(f_0, \varepsilon_1) = \varphi_f (a\varepsilon_1^b) \tag{29}$$

To simplify Eq. (29), we regard parameter b as a constant value, i.e., $b = 1.934$. The specific relationship between D_v and ε_1, and the values of φ_f at each frequency (reference frequency $f_0 = 1\,Hz$) are summarized in Table 1.

Considering the strain amplitude $\varepsilon_r = 0.1\%$ as a reference to normalize the hysteresis loop for other strain amplitudes, D_v/D_{vr} is plotted in Fig. 6. The figure indicates that the hysteresis loss ratio is weakly dependent on frequency, but strongly dependent on $\varepsilon_r/\varepsilon_1$, which is similar to the data in [12]. Assuming that the hysteresis loss ratio is only related to the strain amplitude ratio $\varepsilon_r/\varepsilon_1$, we can express the hysteresis loop D_v as Eq. (30), which is also applicable to [12].

$$D_v(f, \varepsilon_1) = a\left(\frac{\varepsilon_r}{\varepsilon_1}\right)^k D_{vr}(f, \varepsilon_r) \tag{30}$$

Substituting Eq. (28) into Eq. (30), the loss modulus can be derived as

$$E''(f, \varepsilon_1) = a\left(\frac{\varepsilon_r}{\varepsilon_1}\right)^{k+2} E''(f, \varepsilon_r) \tag{31}$$

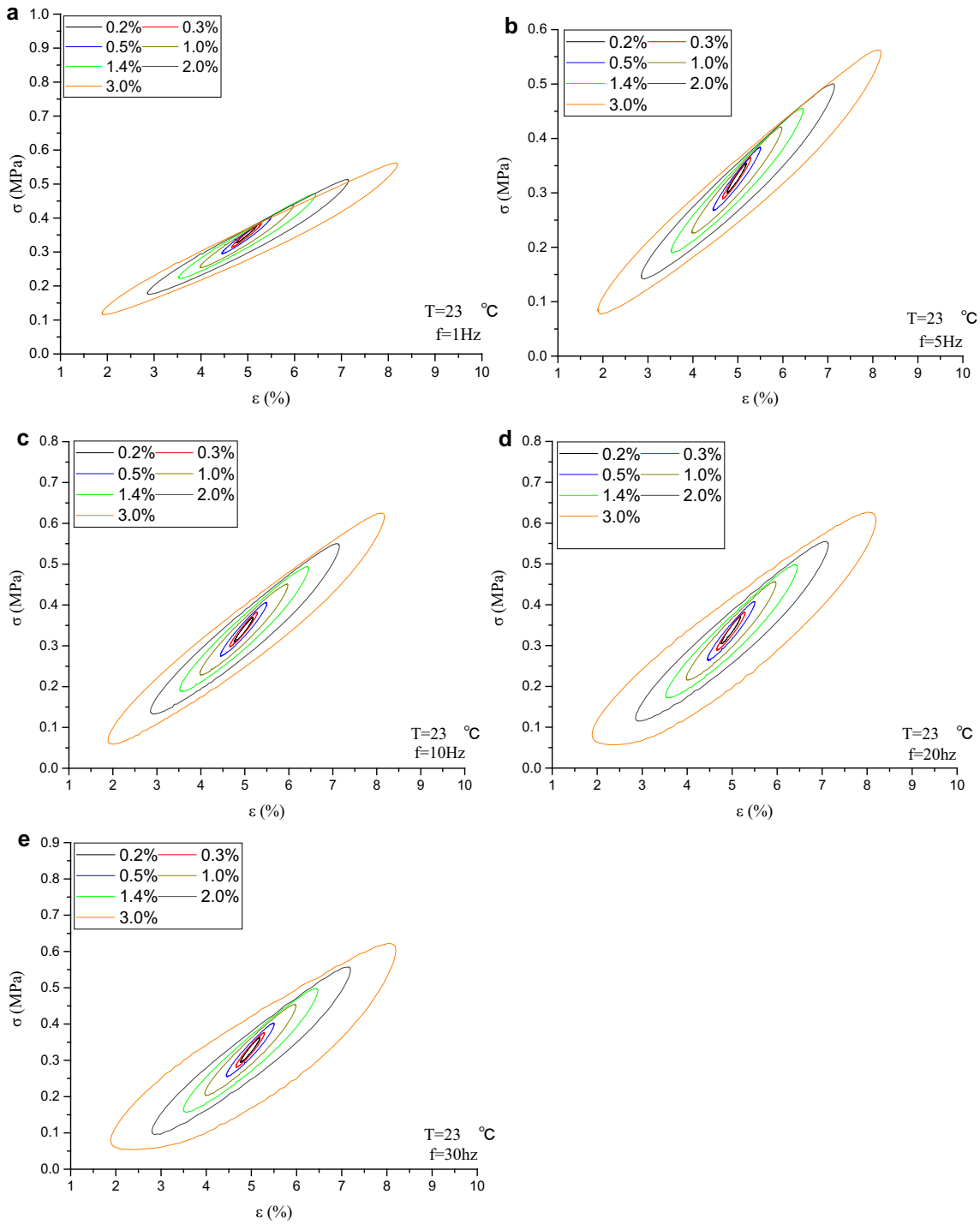

Fig. 4. Hysteresis loops under different frequencies and strain amplitudes

The method of least squares is used for the nonlinear fitting of data in Fig. 6, and the parameters are listed in Table 2. Using Eq. (31), the loss modulus E'' can be predicted when the reference loss modulus is provided, which is often obtained from the frequency sweep test. The reference strain amplitude is selected as $\varepsilon_r = 0.1\%$; and the predicted data at the strain amplitudes of 0.2%, 0.3%, 0.5%, and 1% are displayed in Fig. 7. In comparison with the experimental data of the loss modulus versus frequency,

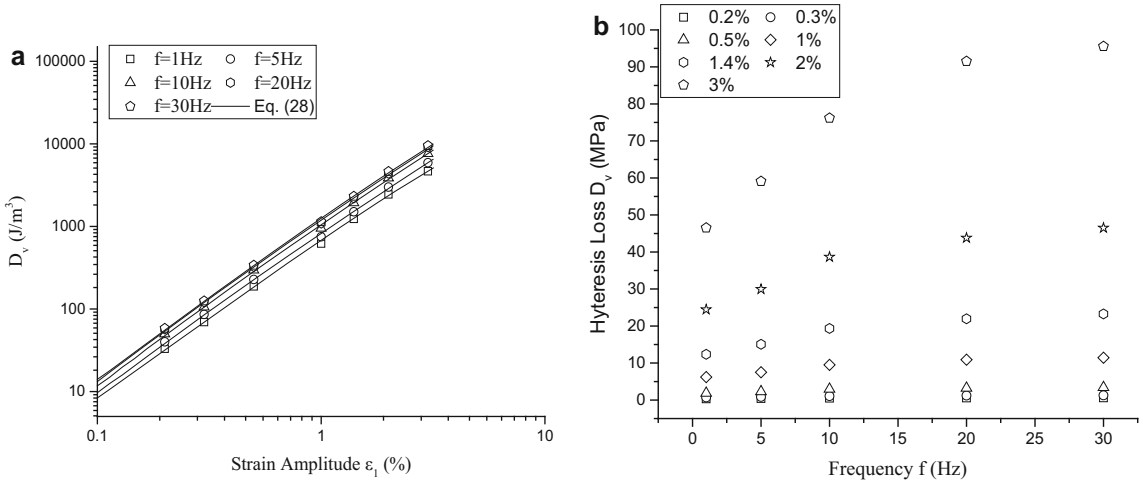

Fig. 5. Hysteresis loss of strain amplitude at specified frequency and strain amplitude

Table 1. **Function of D_v and φ_f at each frequency**

Frequency f (Hz)	$D_v = a\varepsilon_1^{1.934}$	φ_f	$\log \varphi_f$
5	$D_v = 782.7\varepsilon_1^{1.934}$	1.220016	0.086366
10	$D_v = 1008.5\varepsilon_1^{1.934}$	1.549854	0.190291
20	$D_v = 1143.5\varepsilon_1^{1.934}$	1.754727	0.244209
30	$D_v = 1212.8\varepsilon_1^{1.934}$	1.836742	0.264048

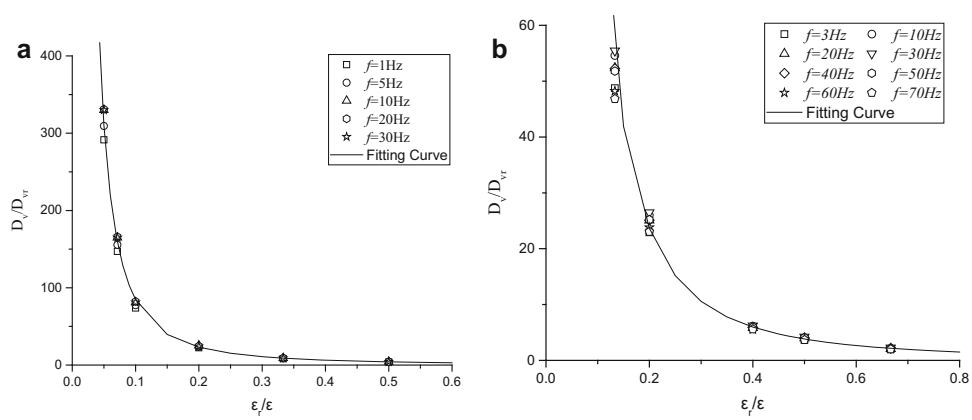

Fig. 6. Experimental data of D_v/D_{vr} (**a** Test data; **b** Literature [12])

Table 2. **Parameters of Eq. (30)**

Parameters	Fitting Value
a	1.065
k	−1.901

a good agreement can be seen between the results, indicating that the empirical formula achieves a good prediction at different strain amplitudes.

In order to determine the accuracy of the predicted results and the experimental data, the variance formula is used.

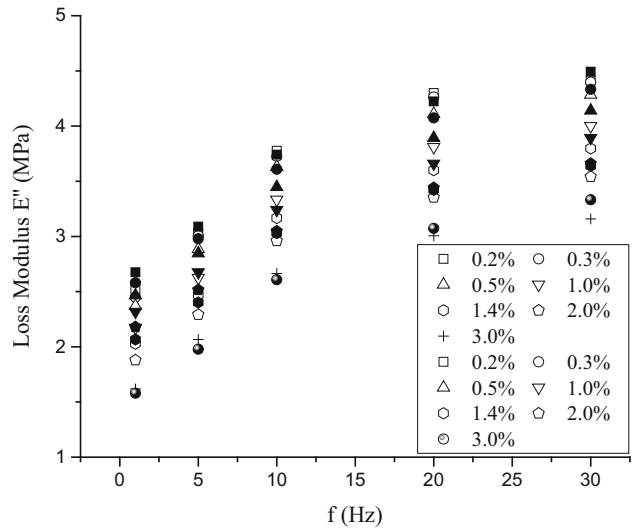

Fig. 7. Fitting results of loss modulus E'' (solid: Prediction; hollow: Test data)

Table 3. ***R*-square between the predicted and experimental results of loss modulus**

Strain amplitude ε_1 (%)	R^2
0.2	0.98
0.3	0.97
0.5	0.96
1.0	0.97
1.4	0.93
2.0	0.91
3.0	0.96

$$R^2 = 1 - \frac{\sum_{n=1}^{N}(E''^2_{\text{pre}} - E''^2_{\text{exp}})}{\sum_{n=1}^{N}(E''^2_{\text{exp}} - \bar{E}''^2_{\text{exp}})} \tag{32}$$

The predicted data and the experimental data are substituted into Eq. (32), and the variance of each strain amplitude is listed in Table 3.

At last, the storage modulus E' is predicted as well. It is not difficult to see from Eq. (27) that the right side is only a polynomial when moving E_0 to the left side. Similarly, we take $\varepsilon_r/\varepsilon$ as the x-axis and $E'-E_0/E'_r-E'_{r0}$ as the y-axis, and the expression takes the form similar to that of Eq. (31).

$$\frac{E'(f,\varepsilon_1)-E_0}{E'(f,\varepsilon_r)-E_{r0}} = \mathrm{b}\left(\frac{\varepsilon_r}{\varepsilon_1}\right)^p \tag{33}$$

By fitting the experimentally measured data of storage modulus E' through the method of least squares, the parameters are determined as $b = 1.1415, p = 0.3163$.

The predicted data for the strain amplitudes $\varepsilon = 0.2\%, 0.3\%, 0.5\%$ and 1% are displayed in Fig. 8a in comparison with the original data of storage modulus E' versus frequency. The variances between the predicted and experimental values of storage modulus are listed in Table 4. The results indicate a good agreement, implying that the empirical formula is effective. Further, Eq. (32) is used to fit the data of storage modulus in [12], which shows a good agreement, as shown in Fig. 8b.

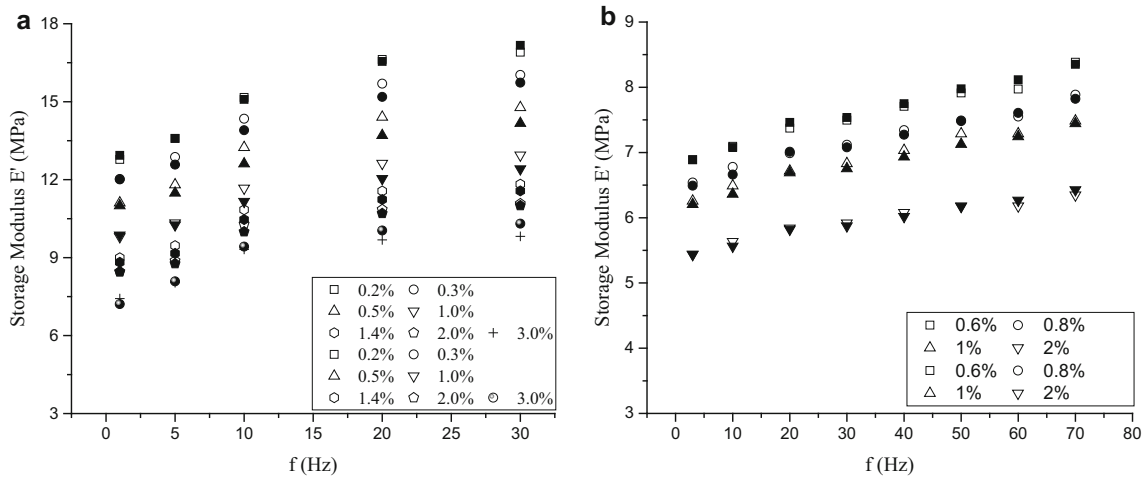

Fig. 8. Fitting results of storage modulus E' (**a** This paper; **b** Literature [12]; solid: Prediction; hollow: Test data)

Table 4. ***R*-square between the predicted and experimental results of storage modulus**

Strain amplitude ε_1 (%)	R^2
0.2	0.99
0.3	0.95
0.5	0.94
1.0	0.98
1.4	0.93
2.0	0.97
3.0	0.91

4. Conclusion

To consider the strain amplitude effect, the superposition of a hyperelastic model and a viscoelastic model was established. The storage modulus and loss modulus were obtained under uniaxial tension, and the model was specified based on the Mooney–Rivlin model and Prony series. An empirical expression was established using the hysteresis loop. A good agreement was observed in comparison with the experimental data of the loss modulus. In addition, the same type of empirical expression was designed, and the fitting results were found to be satisfactory. Moreover, the empirical formula was used to fit the data in the literature, and it proved to be effective. Thus, the empirical formula proposed in this paper, with a simple expression, has certain accuracy in predicting the dynamic modulus under different strain amplitudes.

Acknowledgements. The project was financially supported by the National Natural Science Foundation of China (No. 51708433) and the Fundamental Research Funds. We would like to thank Editage (www.editage.cn) for English language editing.

References

[1] Dai W, Moroni MO, Roesset JM, et al. Effect of isolation pads and their stiffness on the dynamic characteristics of bridges. Eng Struct. 2006;28(9):1298–306.
[2] Siqueira GH, Tavares DH, Paultre P, et al. Performance evaluation of natural rubber seismic isolators as a retrofit measure for typical multi-span concrete bridges in eastern Canada. Eng Struct. 2014;74:300–10.
[3] Yuan Y, Wei W, Tan P, et al. A rate-dependent constitutive model of high damping rubber bearings: modeling and experimental verification. Earthq Eng Struct Dyn. 2016;45(11):1875–92.
[4] Xiang N, Li J. Experimental and numerical study on seismic sliding mechanism of laminated-rubber bearings. Eng Struct. 2017;141:159–74.
[5] Ahmadipour M, Alam MS. Sensitivity analysis on mechanical characteristics of lead-core steel-reinforced elastomeric bearings under cyclic loading. Eng Struct. 2017;140:39–50.

[6] Tinard V, Brinster M, Francois P, et al. Experimental assessment of sound velocity and bulk modulus in high damping rubber bearings under compressive loading. Polym Test. 2018;65:331–8.
[7] Mullins L. Effect of stretching on the properties of rubber. Rubber Chem Technol. 1948;21(2):281–300.
[8] Diani J, Brieu M, Batzler K, et al. Effect of the Mullins softening on mode I fracture of carbon-black filled rubbers. Int J Fract. 2015;194(1):11–8.
[9] Sokolov AK, Svistkov AL, Shadrin VV, et al. Influence of the Mullins effect on the stress-strain state of design at the example of calculation of deformation field in tyre. Int J Nonlinear Mech. 2018;104:67–74.
[10] Payne AR. The dynamic properties of carbon black—natural rubber vulcanizates. Part I. J Appl Polym Sci. 1963;6(19):57–63.
[11] Kraus G. Mechanical losses in carbon-black-filled rubbers. J Appl Polym Symp. 1984;39:75–92.
[12] Luo W, Hu X, Wang C, et al. Frequency-and strain-amplitude-dependent dynamical mechanical properties and hysteresis loss of CB-filled vulcanized natural rubber. Int J Mech Sci. 2010;52(2):168–74.
[13] Lion A, Kardelky C, Haupt P. On the frequency and amplitude dependence of the Payne effect: theory and experiments. Rubber Chem Technol. 2003;76(2):533–47.
[14] Lion A, Kardelky C. The Payne effect in finite viscoelasticity: constitutive modelling based on fractional derivatives and intrinsic time scales. Int J Plast. 2004;20(7):1313–45.
[15] Hofer P, Lion A. Modelling of frequency- and amplitude-dependent material properties of filler-reinforced rubber. J Mech Phys Solids. 2009;57:500–20.
[16] Kim BK, Youn K. A viscoelastic constitutive model of rubber under small oscillatory load superimposed on large static deformation. Arch Appl Mech. 2001;71(11):748–63.
[17] Tomita Y, Azuma K, Naito M. Computational evaluation of strain-rate dependent deformation behavior of rubber and carbon-black-filled rubber under monotonic and cyclic straining. Int J Mech Sci. 2008;50:856–68.
[18] Kar KR, Bhowmick AK. Effect of holding time on high strain hysteresis loss of carbon black filled rubber vulcanizates. Polym Eng Sci. 1998;38(12):1927–45.
[19] Kar KK, Bhowmick AK. Medium strain hysteresis loss of natural rubber and styrene-butadiene rubber vulcanizates: a predictive model. Polymer. 1999;40(3):683–94.
[20] Park DM, Hong WH, Kim SG, et al. Heat generation of filled rubber vulcanizates and its relationship with vulcanizate network structures. Eur Polym J. 2000;36(11):2429–36.
[21] Ismail H, Osman H, Ariffin A. Curing characteristics, fatigue and hysteresis behaviour of feldspar filled natural rubber vulcanizates. J Macromol Sci Part D Rev Polym Process. 2007;46(6):6.
[22] Yang R, Song Y, Zheng Q. Payne effect of silica-filled styrene-butadiene rubber. Polymer. 2017;116:304–13.